Int. J. Electrochem. Sci., 14 **(2019)** 2462 – 2475, doi: 10.20964/2019.03.17

International Journal of
ELECTROCHEMICAL
SCIENCE
www.electrochemsci.org

Short Communication

Preparation of Activated Carbon Electrode from Pineapple Crown Waste for Supercapacitor Application

E. Taer[1,], A. Apriwandi[1], Y. S. Ningsih[1], R. Taslim[2], Agustino[1]*

[1] Department of Physics, University of Riau, 28293 Simpang Baru, Riau, Indonesia
[2] Departement of Industrial Engineering, State Islamic University of Sultan Syarif Kasim, 28293 Simpang Baru, Riau, Indonesia.
[*]E-mail: erman.taer@lecturer.unri.ac.id

Received: 11 November 2018 / *Accepted:* 31 December 2018 / *Published:* 7 February 2019

A pineapple crown activated carbon (PCAC) was prepared from pineapple crown waste using one step carbonisation and physical activation method for electrode super capacitor cells. The pineapple crown waste was also activated by using KOH activation in a ratio of 1 : 1 to the total mass. The pre-carbonised PCAC has a thermal resistance temperature of 300°C while the carbonised one has high Brunauer-Emmett-Teller (BET) with a surface area of 700 m^2g^{-1}, a pore volume of 0.362 m^3g^{-1} and an average pore diameter of 22 nm. The surface morphology of pineapple crown electrode shows a good fibre structure with a diameter of 42-73 nm. The electrochemical properties of supercapacitor cells have an excellent specific capacitance which is as high as 150 F g^{-1} while its energy and power densities are 5.2 Wh Kg^{-1} and 42 W Kg^{-1}, respectively

Keywords: pineapple crown; activated carbon; biomass

1. INTRODUCTION

Indonesia is a pineapple producing country whose production reached 1.73 tonnes in 2015 [1]. The waste products derived from this fruit include leaves and crowns. Their crowns are one of the biomass that contains fiber. The size of the fibers can range from nano to micro meters. The shape of its fiber is one of the most developed forms and this is as a result of several advantages such as hollow pores and good electrical conductivity [2]. Ordinary fiber carbon electrodes are produced from materials like polymers which are highly conductive and can be synthesized through chemical processes. Polymer materials that are usually used are pan, pani and other chemicals which are produced at relatively high costs with relatively limited production rates. Biomass material is a natural material with a structure which is more naturally fibrous than that of cellulose fiber. Various types of

biomass contain cellulose fibers that differ in size and amount in percentage and this enables them to produce varying carbon fiber electrodes at relatively low production costs and unlimited quantities. There have been reports of some biomass materials such as banana fiber [3] and oil palm, empty fruit bunches [4], etc which can be used as originating materials for the preparation of carbon fiber electrodes. Carbon fiber has the advantage of being an electrode in an energy storage device such as an electrochemical double layer capacitor that works based on the principle of ion diffusion into the pore of the electrode.

Energy storage occurs because of the presence of layers of ion and electron which are formed in the micro pore of the carbon electrode. The more the ion pairs and electrons which are formed, the greater the amount of energy that can be stored. The formation of ion and electron pairs is affected by the number of micro pores that are available in an electrode. Micro pore electrodes are related to the materials and their activation process. Besides energy, power is the main factor in the performance of EDLC devices. It is related to the speed at which iron is diffused into the pores of the electrode to form ion-electron pairs. This pace is clearly related to the shape of the electrode constituent material and pore size. Over the last decade, the shape of electrode constituent materials has become a fairly extensive study [5]. In this research, a simple method is used to produce carbon fiber electrodes from pineapple crown waste as super capacitor electrodes. Carbon electrodes are provided without additional adhesives and they are activated conventionally with focus on the difference in CO2 activation at temperatures of 600 °C, 700 °C, 800 and 900 °C. The results showed that the optimum activation temperature at which good physical and electrochemical properties of super capacitor cells were produced is 700 °C. The maximum specific capacitance was as high as 150 F g^{-1} while the dominant carbon fiber had an average diameter size of 68-106 nm.

2. EXPERIMENTAL METHOD

The carbon electrodes of super capacitor from the pineapple crown are produced based on variations in the physical activation temperature. In the first stage, the pineapple crown waste is dried in the sun for 2 days to reduce the moisture content. Pre-carbonization is the process of heating a pineapple crown which is carried out at temperatures ranging from 50ºC to 250°C for a period of 2.5 hours. This process always results in fragility and causes carbon to be blackish. Smoothening the pre-carbonized sample is done by using ballmilling and this produces fine pre-carbonized powder [6,7]. This powder is activated chemically using KOH at a ratio of 1:1, then it is converted to monolith form using hydraulics press [8,9]. The next process is the one-step-pyrolisis [10] which is initiated by carbonization at a temperature ranging from 30°C to 600°C under the N_2 gas environment, and followed by physical activation with the temperature constantly being raised to reach the maximum temperature by flowing CO_2 gas for 2.5 hours. The various temperatures for physical activation are 600°C, 700°C, 800°C and 900°C. To facilitate data analysis, the samples were coded as MN600, MN700, MN800 and MN900 for each physical activation temperature variation. Supercapacitor cells are arranged in the form of a sandwich which consists of two carbon electrodes, two current collectors, electrolytes and a separator, such as we have reported in previous studies [11,12]. The electrolytes

were made from a solution of H_2SO_4 1 M [13] while the separator was made from the membrane of duck eggshells [14].

Several characterisations were carried out on pineapple crown carbon electrodes, namely physical and electrochemical characterisations. The physical properties include calculation of density, thermal resistance of biomass materials, crystallinity properties and surface morphology while the electrochemical ones calculated the specific capacitance using the cyclic voltammetry method.

3. DISCUSSION

3.1. Thermal analysis

Figure 1 shows the TGA measurement of pineapple crown powder which has been pre-carbonized at 250°C. The dashed line is a graph of TG in the percentage of the sample mass shrinkage against the temperature. The graph shows three stages of significant sample mass change, the first stage is a decrease in mass with a percentage of 11.99% from room temperature to a temperature of 261.4°C. The process that occurs is the decomposition of water content accompanied by decomposition of complex compounds such as cellulose [15]. The second stage occurs at temperatures ranging from 261.4°C to 318.7°C with a mass loss of 20.3%. This occurrence is the decomposition of hemicellulose, cellulose, and lignin. The decomposition of hemilose mass reaching 55% occurs at between 200°C and 300°C, cellulose mass loss occurs at temperatures ranging from 260°C to 390°C [16]. That of lignin is quite slow and it starts from a temperature of 160°C to 900°C. The third stage occurs at temperatures ranging from 318.7°C to 489°C with a mass loss of 21.64%. The total mass lost from these two stages is 41.94%.

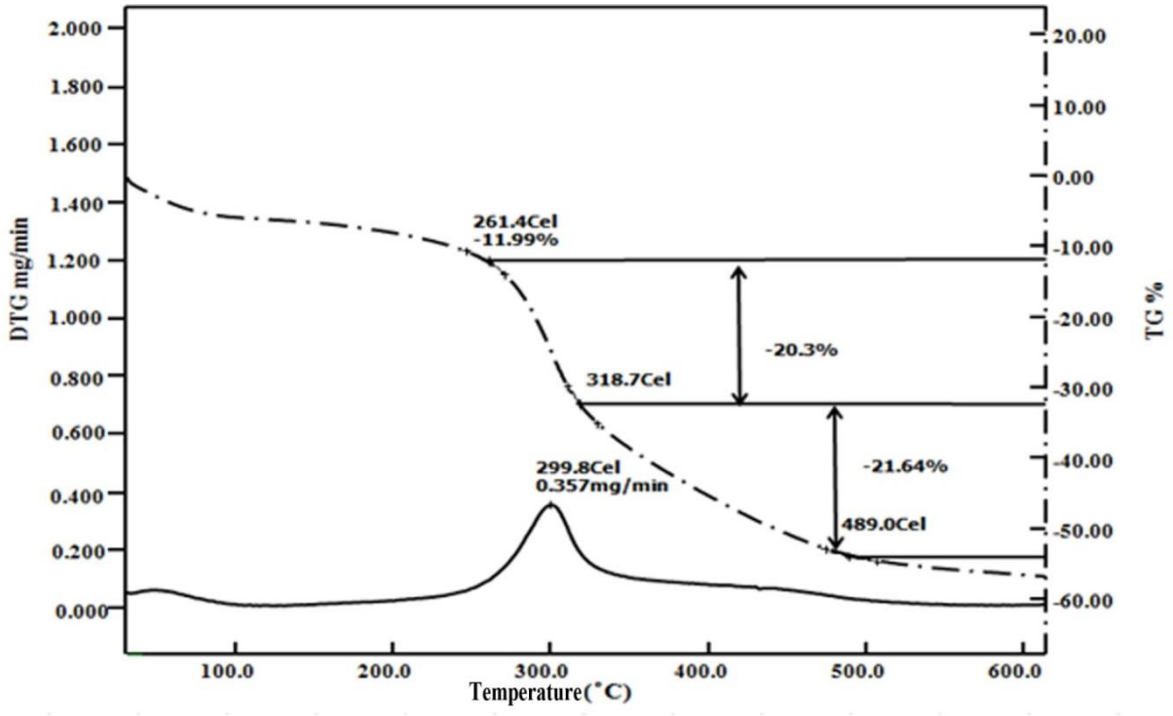

Figure 1. TG and DTG curve for pineapple crown biomass

The remaining sample is carbon material that comes from the pineapple crown. The DTG graph displays the data in form of a straight line that is accompanied by two peaks which determine the maximum mass change rate that occurs in the sample. The decrease in mass from the DTG graph of the time function results in a reduction in weight. The weight loss that occurred in the pineapple crown sample was 0.357mg/min which occurred at a temperature of 299.8°C. At this temperature was select as a thermal resistance in the carbonization process of pineapple crown biomass and hold 1 hour to ensure that this process can occur more perfectly.

3.2. Density analysis

Figure 2 Shows the density of each sample. The data shows that the activation temperature affects the density as an increase in the activation temperature from 600°C to 700°C results in a reduction in density. However, the density increases when the activation temperature is increased to 800°C and 900°C. The pyrolisis process causes the carbon condition to be good (non-carbon components have evaporated from the carbon electrodes), resulting in pores on the electrode and decreased density. The carbonization process can remove impure compounds such as water content, oxygen and Nitrogen. This process leaves holes so that the carbon electrode has a large amount of pores. It leaves an imperfect pore structure so that the physical activation process is needed. Physical activation at 700°C produces the lowest density. This is because at this temperature, it is the optimum condition to remove impurities and rearrange the carbon matrix in the electrode. The phenomenon in this study is similar to that in the previous research [17]. In the process of physical activation, a temperature higher than 700°C demonstrates that the release of impurities is more dominant than the rearrangement of the carbon matrix in the electrode sample, this phenomenon is characterised by a smaller electrode mass which causes the sample density to be higher.

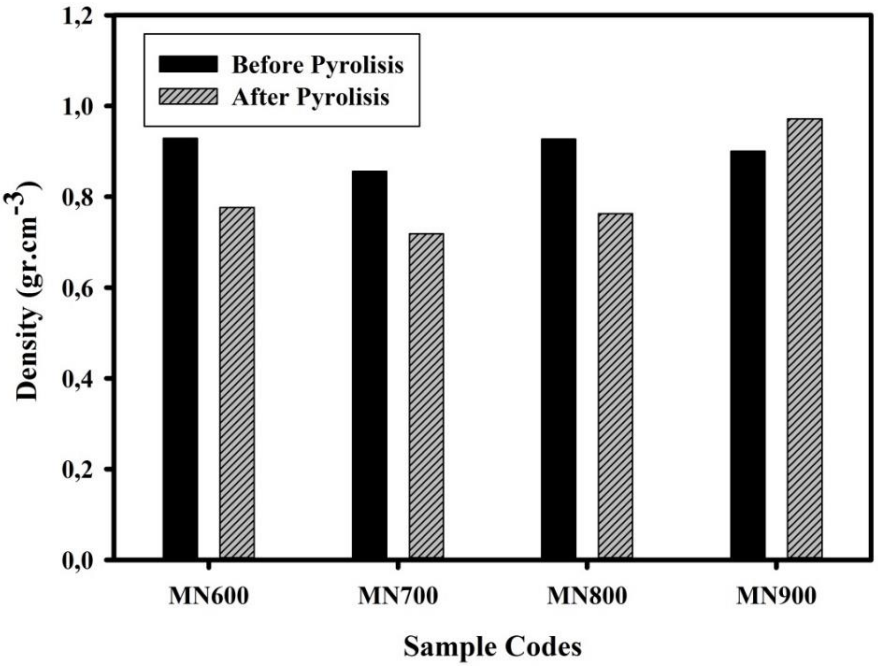

Figure 2. Density of carbon electrode samples

3.3. X-ray Analysis

Figure 3 is a graph of the relationship between X-ray intensity to scattering angle (2θ) in pineapple crown carbon samples. The characterisation results show that there are two wide peaks with an angle of 2θ at 24 and 44 which are related to the diffraction plane (002) and (100) [18]. The determination of 2θ angles for each peak was carried out with help from Microcal Origin software. Data is fitted by using the lorentzian distribution function. The results of the fitting obtained data scattering angle, peak height and peak width. These two peaks indicate that the pineapple crown activated carbon electrode is amorphous.

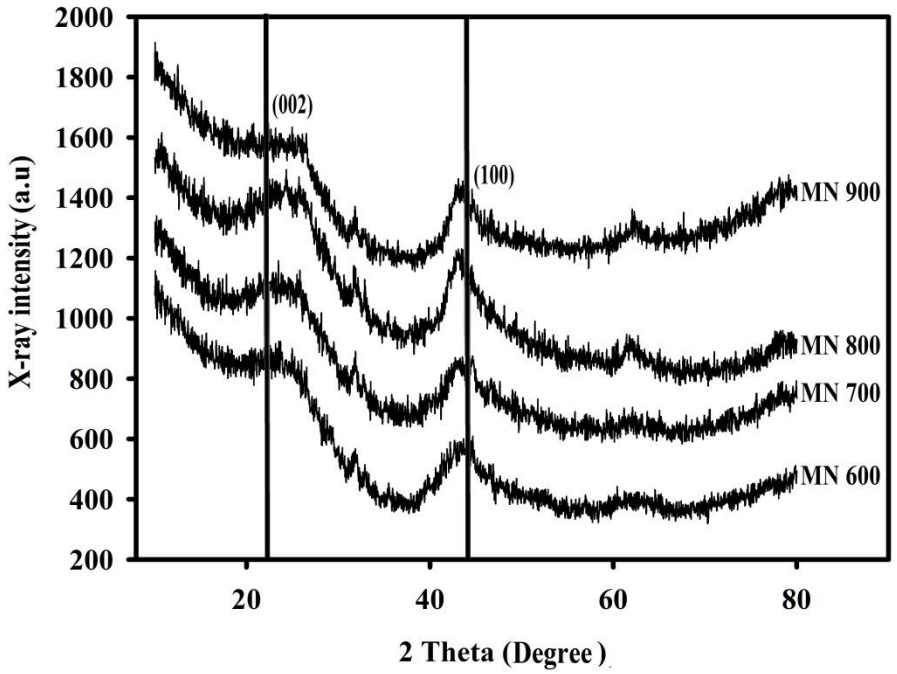

Figure 3. X-ray curve for carbon electrode pineapple crown

Table 1. Data calculation of lattice parameters for monolith pineapple carbon electrodes

Sample codes	$2\theta_{(002)}$ (°)	$2\theta_{(100)}$ (°)	$d_{(002)}$ (Å)	$d_{(100)}$ (Å)	L_c (Å)	L_a (Å)
MN600	24.169	43.986	3.679413	2.056913	12.05188	28.21875
MN700	24.652	44.487	3.608406	2.034904	9.939321	41.65613
MN800	24.564	43.808	3.621134	2.064857	11.50431	44.17795
MN900	24.734	44.001	3.596629	2.056246	11.55130	41.63316

Data calculation of lattice parameters of monolith pineapple carbon electrodes such as peak height (L_c), peak width (L_a) and interlayer spacing (d) are done using the Debye-Scherrer formula [19, 20, 21] and Bragg equation [22], so that the complete data is 2θ, L_c, L_a, and d, as shown in Table 1. It can be seen that the highest L_c is found in the MN600 of 12.05188 Å while the lowest is found in the MN700 sample of 9.939321 Å. The relationship of L_c to surface area is given by the empirical formula

$S=2/\rho_{xrd}L_c$ with ρ_{xrd} being the XRD density which is obtained from $\rho_{xrd}=\{d_{002\ (graphite)}/d_{002}\}\ \rho_{(graphite)}$ with values of $d_{002\ (graphite)}$= 0.33354 nm and $\rho_{(graphite)}$= 2.268 g cm^{-3} [23,24]. Based on the empirical formula, the X-ray diffraction curve data concluded that the smallest surface area is the MN600 sample while the largest is the MN700 sample.

3.3. Surface morfological analysis

Characteristics of Scanning Electron Microscopy (SEM) aim to determine the surface morphological structure of a material. The result of the characterisation of carbon samples from pineapple crown biomass materials is illustrated in Figures 4 and 5.

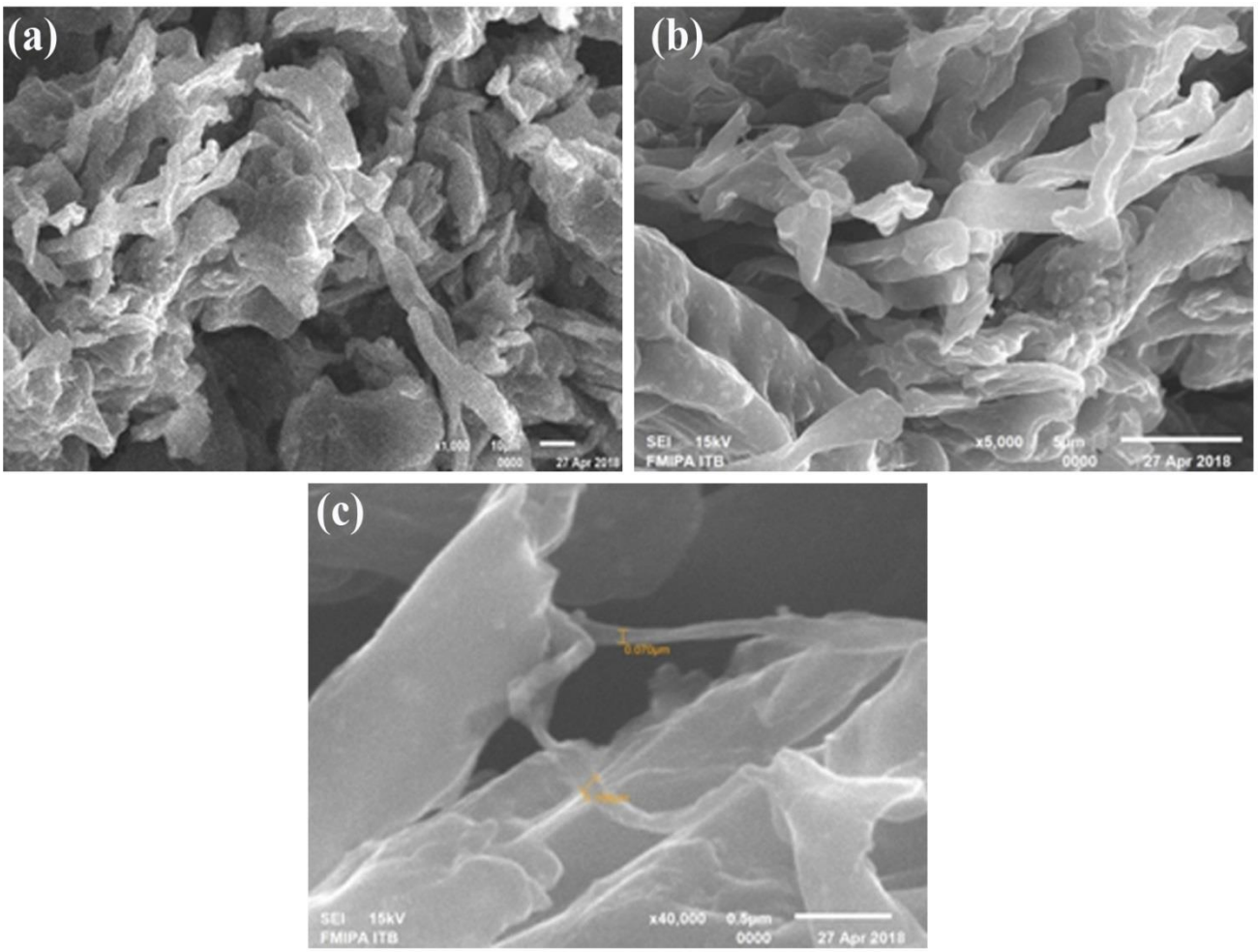

Figure 4. The SEM characterisation for the MN700 sample was carried out using three different magnifications which were a)1000X; b) 5000X and; c) 40000X

Figures 4 and Figure 5 show the surface morphology of carbon electrode for the MN700 and MN900 samples with three different magnifications of 1000X, 5000X, and 40000X. These Figures demonstrate the fiber contained on the surfaces of the two electrode samples. The presence of carbon fiber comes from cellulose fiber that is naturally present in pineapple crown samples. The MN700 at a

magnification of 1000X can be seen in the fiber with a length ranging from 8.643 µm to 14.080 µm and a diameter ranging from 1.019 µm to 1.698 µm. At a 5000X magnification, the presence of fiber is clearer, besides that it also shows the presence of pores formed. This can be seen in Figure 4b where there is a dark pattern between visible fibers. Figure 4c is MN700 with a magnification of 40000X which shows a fiber with a length ranging from 0.641 µm to 1.535 µm and a diameter ranging from 0.070 µm to 0.106 µm.

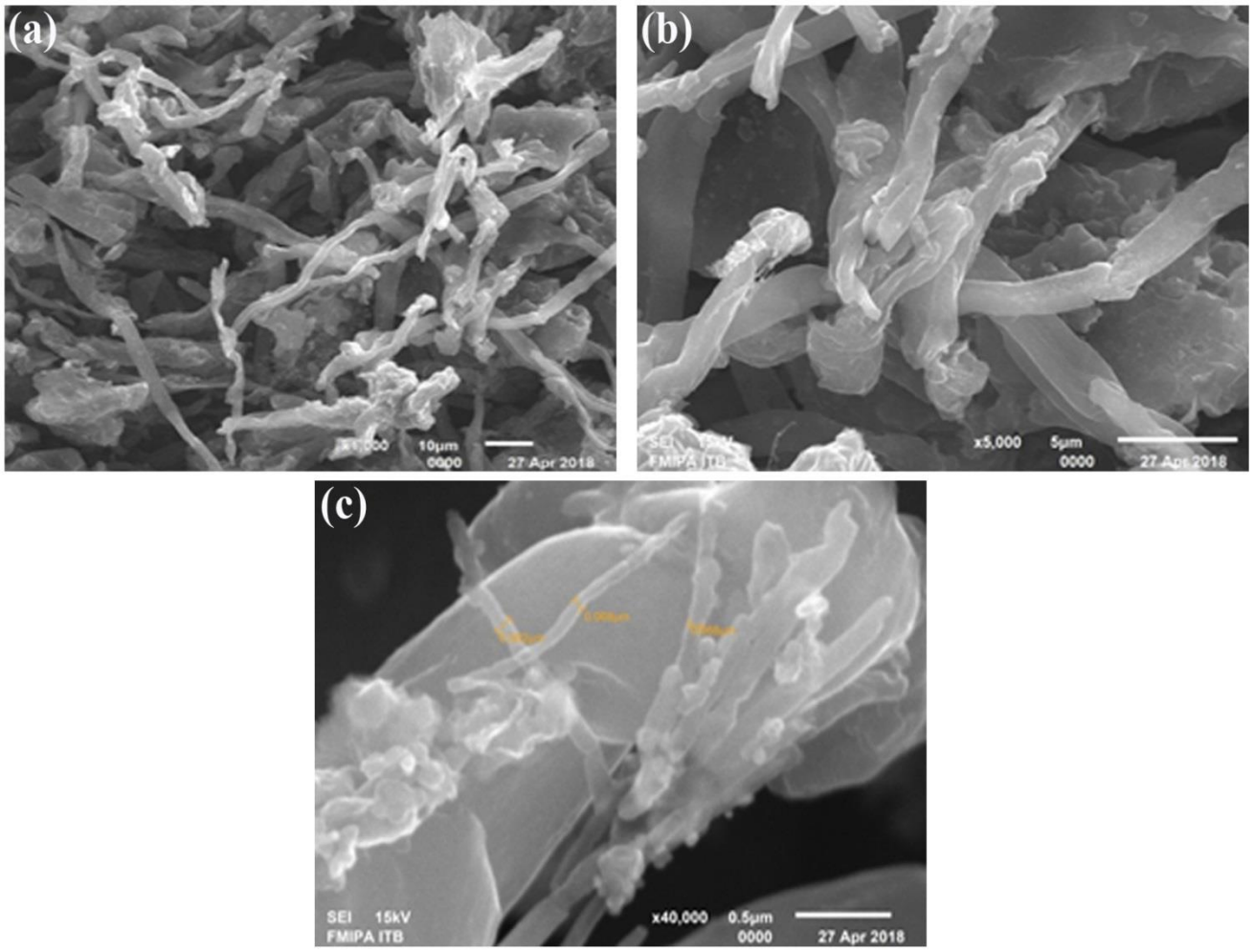

Figure 5. The SEM characterisation for the MN900 sample was carried out using three different magnifications which were a)1000X; b) 5000X and; c) 40000X

Whereas for the MN900 sample, the presence of carbon fiber appears to be more than that of the MN700. At a magnification of 1000X, the MN900 contained fiber with a length ranging from 21.45 µm to 24.90 µm and a diameter ranging from 0.86 µm to 1.84 µm. At a magnification of 5000X, the MN900 fiber is also seen more clearly and at a magnification of 40,000X the fiber length ranged from 0.875 µm to 1.28 µm and the diameters ranged from 0.068 µm to 0.092 µm. This length and diameter range is far greater than that of the carbon fiber in the MN700 sample. This is due to the addition of the physical activation temperature caused by the content of non-carbon being released more and causing clumps between fibers to be released and finally the fiber looks more with finer

diameter sizes. In a study similar to other biomass materials which had nanofiber such as banana stems [25] and mission grass flower [26] with a fiber sizes ranging from 0.042 μm to 0.131 μm and from 0.042 μm to 0.073 μm respectively.

3.4. EDX analysis

The EDX results for pineapple crown carbon electrode samples obtained the elements of Carbon (C), Oxygen (O), Magnesium (Mg), Silicon (Si), and Calcium (Ca). The elemental and atomic content is expressed in percentage and shown in Table 2. The Table shows that higher physical activation temperatures result in a higher purity of carbon in the pineapple carbon crown. The MN700 and MN900 samples have carbon elements that are as high as 89.21% and 93.63%. The resulting carbon content data are similar to that of other studies on bamboo waste [27], banana stem waste [28] and sago waste [29]. The higher the carbon content in a material, the higher the tendency for a good specific capacitance.The MN900 sample has a higher carbon element than the MN700 sample, but the MN900 has a lower specific capacitance than the MN700. This is due to the fact that a high physical activation temperature would eradicate more impurities in the carbon electrode. A lot of impurities ate eradicated, resulting in particles getting denser which causes the flow of ions in the pore to be blocked so that the specific capacitance obtained decreases. This analysis is supported by high MN900 electrode density compared to MN700 electrode density. From Table 2, it can be seen that activated carbon electrode also contains other elements besides carbon, such as oxygen. This is because of the oxygen content left due to incomplete carbonization or bonding which can also occur in the activation process [30]. The weight percentage and the atomic percentage of the MN700 sample are higher than those of the MN900, the percentages are 7.89% and 6.15% for the MN700 sample while for the MN900, they are 6.78% and 5.26%. There are also other elements such as Magnesium (Mg), Silicon (Si) and Calcium (Ca) in the lower percentage.

Table 2. The element contents for MN700 and MN900 samples

Component	**MN700**		**MN900**	
	Weight %	**Atom %**	**Weight %**	**Atom %**
Carbon	89.21	92.63	90.65	93.63
Oxygen	7.89	6.15	6.78	5.26
Magnesium	1.34	0.69	1.42	0.73
Silicon	0.32	0.14	0.29	0.13
Calcium	1.24	0.39	0.86	0.27

3.5. Surface area analysis

Analysis of N_2 gas absorption was carried out at a temperature of 77.350K which gave an isothermal curve between the relative pressure (P/P0) to the STP volume ($cm^3\ g^{-1}$) and this can be seen in Figure 6. The N_2 gas adsorption process occurs at a relative pressure of 0 - 1 then continues with

desorption until it reaches a relative pressure of 0 again. Figure 5 shows that the IUPAC curve formed is the isotherm type II curve [31]. Absorption occurs in mixtures of micropore and mesoporous. Figure 6 shows the amount of gas absorbed by the pineapple carbon related to the relative pressure (P/P0). The pressure is relatively very influential on N_2 gas uptake which enters the pores of the carbon electrode. Figure 6 shows the relationship of absorption volume to changes in N_2 gas pressure. In the MN700 and MN900 curves it is shown that the shape of the hysteresis is in the pressure region of 0.1 to 0.9. The MN900 image shows that the hysteresis curve is not completely formed. It is possible that at a temperature of 900°C, the pore structure of the carbon produced is damaged and as a result of this, the resulting curve is not so good. At the relatively low P/P0 ratio, the formation of micro pores occurs in the carbon sample, then increasing the relative pressure indicates the formation of pores that are larger in the matrix carbon sample [32].

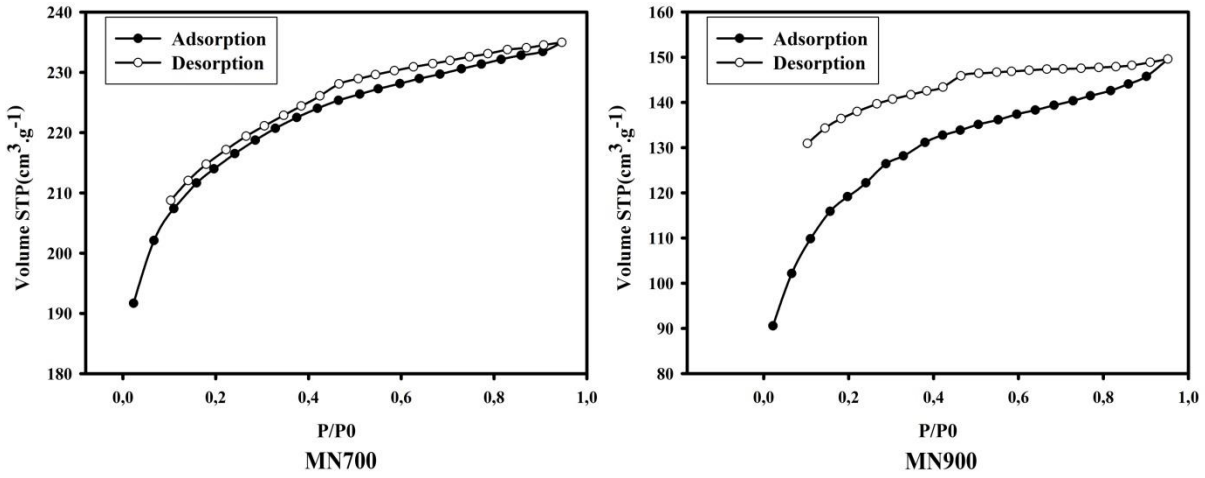

Figure 6. Nitrogen adsorption–desorption isotherms for a) MN700; b) MN900

The Table 3 shows BET surface area (S_{BET}), BJH surface area (S_{BJH}), BET volume (V_{BET}), BJH volume (V_{BJH}), BJH diameter (D_{BJH}) and average pore diameter ($D_{average}$). It also shows the surface area of the sample.

Table 3. BET surface area (S_{BET}), BJH surface area (S_{BJH}), BET volume (V_{BET}), BJH volume (V_{BJH}), BJH diameter (D_{BJH}) and average pore diameter ($D_{average}$) of carbon electrodes using BET characterization

Sample codes	S_{BET} (m^2g^{-1})	S_{BJH} (m^2g^{-1})	V_{BET} (m^3g^{-1})	V_{BJH} (m^3g^{-1})	D_{BJH} (Å)	$D_{average}$ (Å)
MN700	684.035	23.854	0.364	0.0278	35.744	21.308
MN900	39.388	16.866	0.231	0.0189	35.590	23.350

The surface area of the sample tends to decrease with increasing activation temperature. In the table there is also other information like the volume of Barrier Joinet Halenda (VBJH). BJH is a method of measuring the pore structure of activated carbon for micropore and mesoporous sizes [33]. Mesopori is related to power while micropore is related to the energy value of super capacitors [34]. The pore volume for the MN700 sample is 0.364 ($m^3 g^{-1}$) and that for the MN900 sample is 0.231 ($m^3 g^{-1}$). The average pore diameter of the sample for the MN700 code is 21.308 nm while that of the MN900 sample is 23.350nm. According to the IUPAC classification [31], pores are divided into 3 types, namely micropore (d<2nm), mesoporous (2<d>50nm), and macropore (d>50nm). Based on this classification, the pineapple crown carbon electrode sample is dominated by mesopores. Table 4 shows the comparison of the surface areas of different biomasses.

Table 4. Comparison of BET surface areas from different biomasses

Biomass	S_{BET} (m^2g^{-1})	References
Olive residues	771-1390	35
Cattail	441.12	36
Durian shell	467-979	37
Orange peels	300-620	38
Waste tea	1125-1327	39
Coconut shell	1057	40
Pineapple crown	39-700	Present study

3.6. Electrochemical analysis

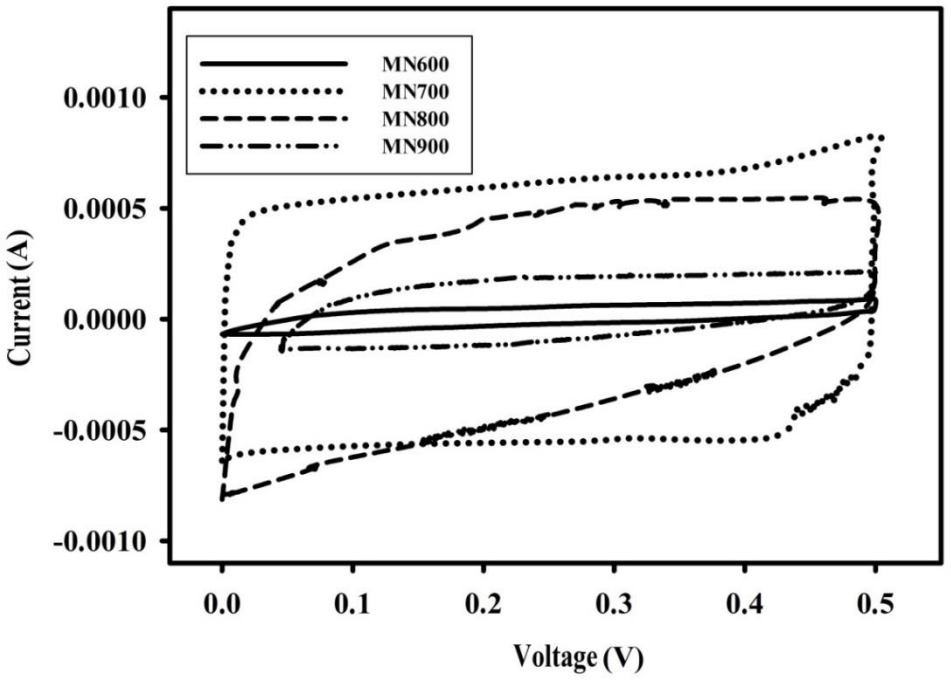

Figure 7. CV curve for all super capacitor cells

Figure 7 is a cyclic voltammogram data that shows the relationship between current and voltage. The charge current (Ic) is shown on the curve from voltage 0 to 0.5 V, while the discharge current (Id) is shown at a voltage of 0.5V to 0. Figure 7 shows the width of the Ic and Id regions. The MN700 cell displays the widest width of the (Ic-Id) area, followed by the MN800, MN900, and MN600 cells respectively. The Ic and Id regions are related to the specific capacitance of the supercapacitor cells [41]. It can be observed that the sequence of specific capacitances from the highest to the lowest in relation to electrode samples are MN700, MN800, MN900, and MN600.

Table 5. Specific capacitances of pineapple crown activated carbon electrodes

Sample codes	Mass (g)	Ic (A)	Id (A)	Specific capacitance (F/g)
MN600	0.00570	0.000052	-0.000015	12
MN700	0.00915	0.000811	-0.000558	150
MN800	0.01115	0.000295	-0.000436	65
MN900	0.00840	0.000188	-0.000099	34

This analysis is in accordance with the specific capacitance data that was obtained using standard formula [42,43] and is completely shown in Table 5. The data presented in Table 5 shows that the MN700 sample has the highest specific capacitance which is as high as 150 F g^{-1} while the MN600 sample shows the lowest which is as high as 12 F g^{-1}. Generally, it can be seen that the increase in activation temperature from 600°C to 700°C results in an increase in the specific capacitance of supercapacitor cell, whereas from 700°C to 900°C, the specific capacitance decreases. 700°C was chosen as the optimum activation temperature, this temperature produced a high pore surface area so that more electrons are trapped inside the pores of the carbon electrode. The maximum capacitance produced in this study is almost the same as the specific capacitance with different biomass materials which shown in Table 6.

Table 6. Comparison of specific capacitance (Csp) of electrodes from different biomass.

Biomass	Csp (F g^{-1})	References
Rice husk & beet sugar	116	[44]
Coffee shell	156	[45]
Coconut husk waste	184	[46]
Waste paper	160	[47]
Paper pulp	166	[48]
Pine-cone	198	[49]
Pineapple leaves	131	[50]
Pineapple leaf fiber	202	[51]
Pineapple crown waste	150	Present study

In addition to specific capacitance, the electrochemical properties of supercapacitors can also be analysed by energy and power densities calculated by standard equations [52,53]. The maximum energy and power densities in this study are 5.2 Wh Kg^{-1} and 42 W Kg^{-1} respectively. These are almost

the same as other supercapacitors with different biomass materials such as olive residues [35], tobacco waste [54] and bamboo [55].

4. CONCLUSION

As a renewable material, the pineapple crown waste successfully fabricated a pineapple crown activated carbon (PCAC) using one step carbonization and physical activation by N_2 and CO_2 gas. The carbon electrode demonstrated good physical properties such as low density, high carbon content and high surface area. Electrochemical cells of electrode from PCAC showed excellent specific capacitance with high energy and power densities. The reported good physical properties and excellent electrochemical performance promises to transform pineapple crown into a good material for the preparation of activated carbon electrode for super capacitor cell.

ACKNOWLEDGEMENTS
The author would like to thank the DRPM Kemenristek-Dikti through the second year Project of PDUPT with the title “Potential of Urban Solid Waste Utilization as a Supercapacitor Electrode” with contract number: 360/UN.19.5.1.3/PP/2018. The author also thanks the SEM FMIPA ITB Laboratory, which has assisted in obtaining the SEM and EDX data.

References

1. E. Respati*, Pusat Data dan Sistem Informasi Pertanian Sekretariat Jenderal Kementerian Pertanian*, (2016) jakarta. Indonesia.
2. L. Yin, Y. Chen, D. Li, X. Zhao, B. Hou, B. Cao, *Mater. Design,* 111 (2016) 44.
3. K. Chaitra, R.T. Vinny, P. Sivaraman, N. Reddy, K. Venkatesh, C. S. Vivek, N. Nagaraju, K. Kathyayini, *J. Energy Chem.,* (2016).
4. M. Deraman, S. K. M. Saad, M. M. Ishak, Awitdrus, E. Taer, I. Talib, R. Omar, M. H. H. Jumali, *the third nanoscale and nanotechnology sympsium* (2014) Malaysia.
5. A. Borenstein, O. Hanna, R. Attias, S. Luski, T. Brousse, D. Aurbach, *J. Mater. Chem.,* 5 (2017) 12653.
6. N. S. M. Nor, M. Deraman, R. Omar, E. Taer, Awitdrus, R. Farma, N. H. Basri, B. N. M. Dola, *AIP Conf. Proc.*, 1586 (2014) 68.
7. E. Taer, M. Deraman, I. A. Talib, S. A. Hashmi, A. A. Umar, *Electrochim. Acta*, 56 (2011) 10217.
8. E. Taer, P. Dewi, Sugianto, R. Syech, R. Taslim, Salomo, Y. Susanti, A. Purnama, Apriwandi, Agustino, R. N. Setiadi, *AIP Conf. Proc.,* 1927 (2018) 030026-1.\
9. E. Taer, B. Kurniasih, F. P. Sari, Zulkifli, R. Taslim, Sugianto, A. Purnama, Apriwandi, Y. Susanti, *AIP Conf. Proc.,* 1927 (2018) 030006-1.
10. E. Taer, Apriwandi, Yusriwandi, W. S. Mustika, Zulkifli, R. Taslim, Sugianto, B. Kurniasih, Agustino, P. Dewi, AIP Conf. Proc. 1927 (2018) 030036-1.
11. M. Deraman, R. Omar, S. J. Zakaria, *J. Mater. Sci.,* 7 (2002) 3329.
12. R. Farma, M. Deraman, A. Awitdrus, I. A. Talib, E. Taer, J. G. Manjunatha, M. M. Ishak, B. N. M. Dollah, S. A. Hashmi, N. H. Basri, *Bioresource Technology,* 132 (2013) 254.
13. Iwantono, E. Taer, A. A. Umar, *AIP Conf. Proc.,* 1454 (2012) 251.

14. E. Taer, Sugianto, M. A. Sumantre, R. Taslim, Iwantono, D. Dahlan, M. Deraman, *Adv. Mater. Research,* 896 (2014) 66.
15. L. L. Zhang, S. X. Zhao, *Chemical Society Reviews,* 38 (2009) 2520.
16. M. Brebu, C. Vasile, *Cellulose Chemistry Technology,* 49 (2010) 353.
17. E. Taer, A. Afrianda, R. Taslim, Krisman, Minarni, A. Agustino, U. Malik, A. Apriwandi, *J. Phys.: Conf. Ser.* 1120 (2018) 012007.
18. G. Yu, L. Lei, J. Yuming, W. Yu, Y. Chuanjun, W. Yingjin, C. Gang, G. Junjie, L. Haiyan, *Appl. Energy,* 153 (2015) 41.
19. B. D. Cullity, Elements of X-Ray Diffraction, Ed. 3, (2001) Amazon Prentice Hall.
20. J. M. V. Nabais, J. G. Teixeira, I. Almeida, *Bioresour. Technol.,* 102 (2010) 2781.
21. Awitdrus, M. Deraman, I.A. Talib, R. Omar, M.H. Jumali, E. Taer, M.H. Saman, *Sains Malaysiana,* 39 (2010) 83.
22. A. González, E. Goikolea, J.A. Barrena, R. Mysyk, *Renewable and Sustainable Energy Reviews,* 58 (2016) 1189.
23. K. Kumar, R. K. Saxena, R. D. Kothari, K. Suri, N. K. Kaushik, J. N. Bohra, *Carbon,* 35 (1997) 1842.
24. M. Deraman, R. Daik, S. Soltaninejad, N. S. M. Nor, Awitdrus, R. Farma, N. F. Mamat, N. H. Basri, M. A. R. Othman, *Adv. Materials Research,* 1108 (2015) 1.
25. E. Taer, R. Taslim,W.S. Mustika, B. Kurniasih, Agustino, A. Afrianda, Apriwandi, *Int. J. Electrochem. Sci.,* 13 (2018) 8428.
26. Zulkifli, Awitdrus, E. Taer, *J. Aceh Phys. Soc.,* 7, (2018) 30.
27. Y. Z. Zhang, Z. J. Xing, Z. K. Duan, M. Li, Y. Wang, *Applied Surface Science,* 315 (2014) 279.
28. E. Taer, Y. Susanti, Awitdrus, Sugianto, R. Taslim, R. N. Setiadi, S. Bahri, Agustino, P. Dewi, B. Kurniasih, *AIP Conf. Proc.,* 1927 (2018) 030016-1.
29. E. Taer, A. Afrianda, Apriwandi, R. Taslim, A. Agustino, Awitdrus, and R. Farma, *Int. J. Electrochem. Sci.,* 13 (2018) 10688.
30. H. Jankowski, A. Swiatkowski, J. Choma, Active Carbon, Ellis Horwood, (1991) London.
31. W. S. K. Sing, H. D. Everett, W. A. R. Haul, L. Moscou, A. R. Pierotti, J. Rouquerol, T. Siemieniewska, *Pure & App. Chem.,* 57 (1985) 603.
32. W. R. Li, D. H. Chen, Z. Li, Y. F. Shi, Y. Wan, G. Wang, Z. Y. Jiang, D. Y. Zhao, *Carbon,* 45 (2007) 1757.
33. X. Wu, X. Hong, Z. Luo, K.S. Hui, H. Chen, J. Wu, K.N. Hui, L. Li, J. Nan, Q. Zhang, *Electrochim. Acta,* 89 (2013) 400.
34. J. S. Huang, B. G. Sumpter, V. Meunier, Angewandte Chemie International Ed 47 (2008) 520.
35. A. Elmouwahidi, E. Bailon-Garcia, A. F. Perez-Cadenas, F. J. Maldonado-Hodar, F. Carrasco-Marin, *Electrochim. Acta,* 229 (2017) 219.
36. M. Yu, Y. Han, J. Li, L. Wang, *Chemical Engineering Journal,* 317 (2017) 493.
37. T. C. Chandra, M. M. Mirna, J. Sunarso, Y. Sudaryanto, S. Ismadji, *J. Taiwan Institute of Chemical Engineers*, 40 (2009) 457.
38. M. E. Fernandez, B. Ledesma, S. Román, P. R. Bonelli, A. L. Cukierman, *Bioresource Technology*, 183 (2015) 221.
39. I. I. G. Inal, S. M. Holmes, A. Banford, Z. Aktas, *Applied Surface Science,* 357 (2015) 696.
40. J. Katesa, S. Junpirom, C. Tangsathitkulchai, *TIChE International Conference 2011,* November 10 – 11, 2011 at Hatyai, Songkhla Thailand.
41. E. J. Ra, E. Raymundo-Piñero, Y. H. Lee, F. Béguin, *Carbon,* 47 (2009) 84.
42. L. Li, E. Liu, J. Li, Y. Yang, H. Shen, Z. Huang, X. Xiang, W. Li, *Journal of Power Sources,*195 (2010) 1516.
43. L. Q. Mai, A. Minhas-Khan, X. C. Tian, K. M. Hercule, Y. L. Zhao, X. Lin, X. Xu, *Nat. Commun.,* 4 (2013) 1.
44. S. Kumagai, M. Sato, D. Tashima, *Electrochim. Acta*, 114 (2013) 617.

45. M. R. Jisha, Y. J. Hwang, J. S. Shin, K. S. Nahm, T. P. Kumar, K. Karthikeyan, N. Dhanikaivelu, D. Kalpana, N. G. Renganathan, A. M. Stephan, *Material Chemistry and Physics*, 115 (2009) 33.
46. E. Taer, R. Taslim, A. W. Putri, A. Apriwandi, A. Agustino, *Int. J. Electrochem. Sci.,* 13 (2018) 12072.
47. D. Kalpana, S. H. Cho, S. B. Lee, Y. S. Lee, R. Misra, N. G. Renganathan*, J .Power Sources,* 190 (2009) 587.
48. H. Wang, Z. Li, J. K. Tak, C. M. B. Holt, X. Tan, Z. Xu, B. S. Amirkhiz, D. Harfield, A. Anyia, T. Stephenson, D. Mitlin, *Carbon*, 57(2013) 317.
49. K. Karthikeyan, S. Amaresh, S. N. Lee, X. Sun, V. Aravindan, Y-G. Lee, Y. S. Lee, *ChemSusChem*, 7(2014) 1435.
50. J. Sodtipinta, T. Amornsakchai, P. Pakawatpanurut, *Adv. Nat. Sci.: Nanosci. Nanotechnol,* 8 (2017) 035017.
51. J. Sodtipinta, C. Ieosakulrat, N. Poonyayant, P. Kidkhunthod, N. Chanlek, T. Amornsakchai, P. Pakawatpanurut*, Ind. Crops Prod.,* 104 (2017) 13.
52. S. Faraji, F. N. Ani, *Renew. Sust. Energ. Rev.,* 42 (2015) 823.
53. Y. Zhang, X. J. Li, J. F. Huang, W. Xing, Z. F. Yan, *Nanoscale Res. Lett.,* 11 (2016) 163.
54. H. Chen, Y-C. Guo, F. Wang, G. Wang, P-R.Qi, X-H. Guo, B. Dai, F. Yu, *New Carbon Materials,* 32 (2017) 592.
55. G. Zhang, Y. Chen, Y. Chen, H. Guo, *Materials Research Bulletin,* 102 (2018) 391.